PRIFYSGOL ABERYSTWYTH UNIVERSITY

Aberystwyth University

Stability of a helicoidal surface inside a cylinder with pinned diameters

Whittaker, Robert J.; Cox, Simon

Published in:
Quarterly Journal of Mechanics and Applied Mathematics

DOI:
10.1093/qjmam/hbu026

Publication date:
2015

Citation for published version (APA):
Whittaker, R. J., & Cox, S. (2015). Stability of a helicoidal surface inside a cylinder with pinned diameters. *Quarterly Journal of Mechanics and Applied Mathematics*, *68*(1), 23-52. https://doi.org/10.1093/qjmam/hbu026

General rights
Copyright and moral rights for the publications made accessible in the Aberystwyth Research Portal (the Institutional Repository) are retained by the authors and/or other copyright owners and it is a condition of accessing publications that users recognise and abide by the legal requirements associated with these rights.

• Users may download and print one copy of any publication from the Aberystwyth Research Portal for the purpose of private study or research.
• You may not further distribute the material or use it for any profit-making activity or commercial gain
• You may freely distribute the URL identifying the publication in the Aberystwyth Research Portal

Take down policy
If you believe that this document breaches copyright please contact us providing details, and we will remove access to the work immediately and investigate your claim.

tel: +44 1970 62 2400
email: is@aber.ac.uk

Download date: 30. Aug. 2021

STABILITY OF A HELICOIDAL SURFACE INSIDE A CYLINDER WITH PINNED DIAMETERS

by ROBERT J. WHITTAKER

(*School of Mathematics, University of East Anglia, Norwich Research Park, Norwich, NR4 7TJ, UK.*)

and SIMON COX

(*Department of Mathematics and Physics, Aberystwyth University, Aberystwyth, Ceredigion, SY23 3BZ, UK.*)

[Under consideration for publication in *Q. J. Mech. Appl. Math.*]

Summary

A mathematical analysis is presented of the stability of a soap film with uniform surface tension when stretched between two diameters on the inside of a circular cylinder. The stability boundary is found as a critical twist angle θ between the two diameters, as a function of the aspect ratio ℓ of the cylinder. Numerical and asymptotic results agree well with previous numerical simulations and experiments by Cox & Jones (*J. Engr Math*, 2014, **86**, 1–7). Their hypothesis that the stability boundary for the multiple-vane case is identical to the single film case is confirmed. It is also shown that two distinct instability mechanisms operate. For moderate and small θ/ℓ, the instability is driven by the decrease in area caused by the film moving to an off-diameter position. But for larger θ/ℓ (more twisted films), the decrease in area is dominated by an internal rearrangement of the surface. The latter mechanism is more relevant to Plateau borders in foams, and our results indicate that straight Plateau borders should be stable at any length provided the total twist is less than $\pi/\sqrt{2}$.

1. Introduction

Surface-tension-driven interfaces that attempt to minimize their surface area are common in situations involving two immiscible fluids. In many cases, such as in liquid foams, there will be multiple such surfaces interacting with one another. Plateau first laid down what are now know as 'Plateau's laws' for static configurations of interacting soap films (**1**). Apart from at interfaces, the films are smooth surfaces, and each smooth piece has a uniform curvature. The films meet in lines (known as Plateau borders), with three films meeting at equally spaced 120° angles. The lines meet in fours at isolated vertices, which have tetrahedral symmetry. These laws were subsequently proved by Taylor (**2**) using differential-geometry methods.

While Plateau's laws give necessary conditions for static equilibrium, the problem of understanding dynamical behaviour and the instabilities that lead to topological changes is more challenging. A review by Weaire *et. al.* (**3**) describes various instabilities in liquid foams and the topological changes that can result. Here, we present a mathematical analysis of one instability that is relevant to Plateau borders that are subjected to a twist.

Recently, Cox & Jones (**4**) studied the stability of a soap film inside a circular cylinder,

 © Oxford University Press ????

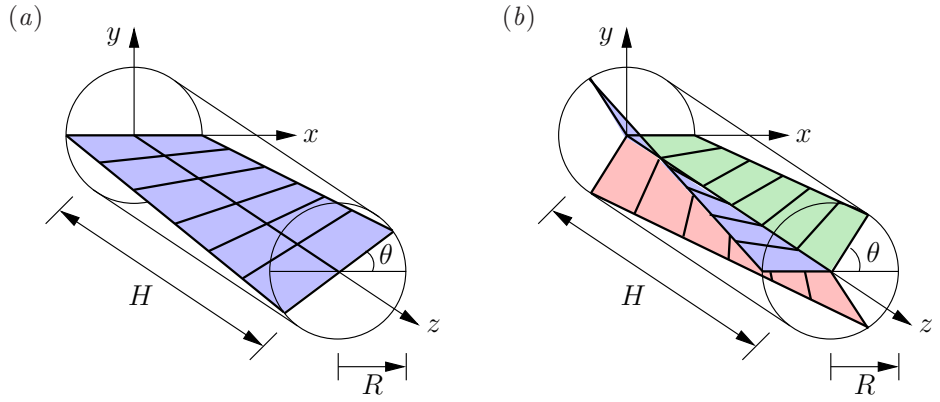

Fig. 1 The Cartesian coordinate system (x, y, z) and the cylinder of radius R and length H that contains the initial helicoidal surface. In the single-vane case (a), the surface is pinned between two diameters at each end with a relative twist θ. In the multiple-vane case (b), N vanes ($N = 3$ is illustrated) are pinned between equally spaced radii at each end, all with the same twist θ between the two ends.

by conducting experiments and numerical simulations using *Surface Evolver* (**5**). They began by considering an initially helicoidal surface that is pinned between two diameters a distance H apart and twisted by an angle θ. The other two edges of the film make contact with the curved wall of the cylinder, which has radius R. See Fig. 1(a). The area of this helicoidal surface is stationary with respect to small perturbations, but was found to be either stable or unstable depending on the values of θ and $\ell \equiv H/R$. Experimentally and numerically, Cox & Jones started from (smaller) values of θ and ℓ where the surface was stable, and increased one or other variable until the surface became unstable. (The instability typically manifested itself by the film bending axially off the diameter, the two sides along the cylinder wall meeting, and then the film separating into two and collapsing back to a semicircle at each end.)

Cox & Jones (**4**) went on to consider the case of multiple vanes pinned between equally spaced radii and joined at a central singular line (a Plateau border in the case of three vanes) that initially lay along the axis of the cylinder. See Fig. 1(b). The stability boundary they obtained in θ–ℓ space appeared to be the same for both the single and all multiple-vane cases. In addition, they also presented an analytical theory for the stability of a single initially flat film ($\theta = 0$) as ℓ is varied.

In this paper, we extend the analytic theory to the case of twisted films. We adopt the same approach as that used by Cox & Jones (**4**); namely seeking perturbations that minimize the area with respect to other nearby perturbations. These perturbations will represent the most energetically favourable deformation. At the stability boundary, one such perturbation will have precisely zero change in area from the original surface. For on one side of the boundary, all perturbations must have a strictly large area, whereas on the other, at least one perturbation must result in a strictly smaller area.

In §2 we set up the mathematical description for the single film case, and obtain the equations that describe an area-minimizing perturbation. We show that the perturbation

can be decomposed into axial Fourier and radial parity modes, and that the area of the perturbed surface can be written as the sum of the area changes due to each of the modes. In §3 we show that the behaviour of the fundamental even mode governs the stability of the film. From the numerical solution of a second-order ODE, we are able to compute the critical mode and the location of the stability boundary.

We also investigate the physical mechanisms that lead to the instability. We find that for moderate twists θ, the instability arises due to the perturbed surface being able to reduce its area by moving its contact line with the curved cylindrical walls. For larger θ a second mechanism, involving an internal rearrangement of the surface near the axis also operates. For $\theta > \pi/\sqrt{2}$, we show that this second mechanism can lead to instability in the absence of area saving by the curved walls.

In §4, we extend our analysis to multiple vanes and show that for any number of vanes, the problem can be reduced to the same equations as for the single-film problem. The problems therefore all have precisely the same stability boundary in θ–ℓ space. Finally, we present our conclusions in §5.

2. Mathematical Formulation

The soap-film surface is modelled as a deformable membrane with uniform surface tension and no resistance to bending or shearing. It therefore seeks to minimize its total area.

2.1 *Initial surface and perturbation*

We use Cartesian coordinates (x, y, z), and consider an initially helicoidal surface bounded by the interior wall of a cylinder at $x^2 + y^2 = R^2$ and pinned to two diameters at $z = 0$ and $z = H$. The diameter at $z = H$ is rotated by an angle θ about the z axis relative to the diameter at $z = 0$, giving the surface a twist as shown in Fig. 1(a). Without loss of generality, we take $R > 0$, $H > 0$ and $\theta \geq 0$.

We non-dimensionalize lengths on the cylinder radius R, and define $\ell = H/R$ as its dimensionless length (or aspect ratio). The initial helicoid surface is then described by specifying the non-dimensional position $\boldsymbol{x_0}$ of a general point on the surface in terms of two dimensionless coordinates $\xi \in (-1, 1)$ and $\eta \in (0, \ell)$:

$$\boldsymbol{x}_0(\xi, \eta) = \begin{pmatrix} \xi \cos k\eta \\ \xi \sin k\eta \\ \eta \end{pmatrix}, \tag{2.1}$$

where $k = \theta/\ell$ is the helicity or pitch parameter. See Fig. 2(a).

By considering the vector cross product $(\partial \boldsymbol{x}_0/\partial \xi) \times (\partial \boldsymbol{x}_0/\partial \eta)$, the unit normal to this surface is found to be

$$\hat{\boldsymbol{n}} = \frac{1}{(1 + k^2\xi^2)^{1/2}} \begin{pmatrix} -\sin k\eta \\ \cos k\eta \\ -k\xi \end{pmatrix}. \tag{2.2}$$

We then describe a general perturbation to the surface using a small parameter $\epsilon \ll 1$ and a function $\zeta(\xi, \eta)$, such that $\epsilon\zeta$ is the normal displacement from each point of the original

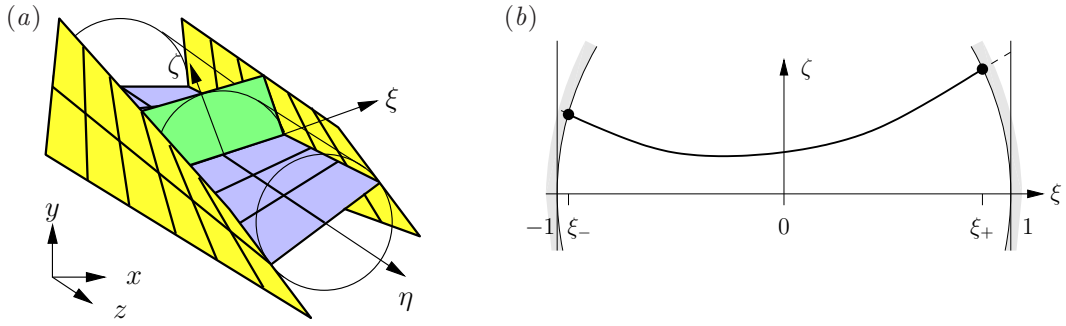

Fig. 2 The geometry and coordinates associated with the initial helicoid surface and its deformations. (a) The initial surface $\boldsymbol{x}_0(\xi,\eta)$ parameterised by coordinates ξ and η. The surfaces formed by the normals $\hat{\boldsymbol{n}}$ at the cylinder walls ($\xi=\pm1$) are also shown, as is a ξ–ζ surface generated by normals at a fixed η. (b) The deformations within a ξ–ζ surface, showing how the converging cylinder walls cause the range of ξ to be diminished from $(-1,1)$ to $(\xi_-(\eta),\xi_+(\eta))$.

surface. The new surface is thus given parametrically by

$$\begin{aligned}\boldsymbol{x}(\xi,\eta) &= \boldsymbol{x}_0(\xi,\eta) + \epsilon\,\zeta(\xi,\eta)\,\hat{\boldsymbol{n}}(\xi,\eta)\\ &= \begin{pmatrix}\xi\cos k\eta\\ \xi\sin k\eta\\ \eta\end{pmatrix} + \frac{\epsilon\,\zeta(\xi,\eta)}{(1+k^2\xi^2)^{1/2}}\begin{pmatrix}-\sin k\eta\\ \cos k\eta\\ -k\xi\end{pmatrix}.\end{aligned} \tag{2.3}$$

The pinned diameters at $z=0,\ell$ require that we take

$$\zeta(\xi,0)=\zeta(\xi,\ell)=0\,. \tag{2.4}$$

Owing to the curvature of the cylinder walls, the outer edges of the deformed surface will no longer occur precisely at $\xi=\pm1$. See Fig. 2(b).

2.2 *Area of the perturbed surface*

The area of the perturbed surface is given by

$$\mathscr{A}=\int_0^\ell\int_{\xi_-(\eta)}^{\xi_+(\eta)}\mathscr{L}(\xi,\eta;\zeta)\,\mathrm{d}\xi\,\mathrm{d}\eta\,, \tag{2.5}$$

where $\xi_\pm(\eta)$ are the values of ξ at which the perturbed surface meets the cylinder wall, and

$$\mathscr{L}=\left|\frac{\partial\boldsymbol{x}}{\partial\xi}\times\frac{\partial\boldsymbol{x}}{\partial\eta}\right| \tag{2.6}$$

is the surface area per unit coordinate area.

The points $\xi_\pm(\eta)$ are found using

$$\Big(\boldsymbol{x}(\xi_\pm,\eta)\cdot(1,0,0)^T\Big)^2+\Big(\boldsymbol{x}(\xi_\pm,\eta)\cdot(0,1,0)^T\Big)^2=1\,. \tag{2.7}$$

Substituting from (2.3) we obtain (without approximation)

$$\xi_\pm^2 = 1 - \frac{\epsilon^2 \big[\zeta(\xi_\pm,\eta)\big]^2}{1+k^2\xi_\pm^2}\,. \tag{2.8}$$

So $\xi_\pm = \pm 1 + O(\epsilon^2)$, and thence by expanding the right-hand side of (2.8) in powers of ϵ, we obtain

$$\xi_\pm = \pm\left(1 - \frac{\epsilon^2\zeta_\pm^2}{2(1+k^2)}\right) + O(\epsilon^4)\,, \tag{2.9}$$

where $\zeta_\pm = \zeta(\pm 1,\eta)$.

We evaluate $\mathscr{L}$ from the expression for $\boldsymbol{x}(\xi,\eta)$ in (2.3). Expanding in powers of ϵ, we obtain

$$\mathscr{L} = \mathscr{L}_0 + \epsilon^2\mathscr{L}_2 + O(\epsilon^3)\,, \tag{2.10}$$

where

$$\mathscr{L}_0(\xi) = \big(1+k^2\xi^2\big)^{1/2}\,, \tag{2.11}$$

$$\mathscr{L}_2(\xi,\eta;\zeta) = \frac{1}{2}\big(1+k^2\xi^2\big)^{1/2}\left(\frac{\partial\zeta}{\partial\xi}\right)^2 + \frac{1}{2}\big(1+k^2\xi^2\big)^{-1/2}\left(\frac{\partial\zeta}{\partial\eta}\right)^2 - \big(1+k^2\xi^2\big)^{-3/2}k^2\zeta^2\,. \tag{2.12}$$

There is no $O(\epsilon)$ term in the expansion (2.10) because the area of the original helicoid surface is stationary with respect to small perturbations.

Using the expressions (2.9) and (2.10)–(2.12), We can now write the area (2.5) as

$$\mathscr{A} = \mathscr{A}_0 + \epsilon^2\left(\mathscr{A}_2^{(s)} + \mathscr{A}_2^{(w)}\right) + O(\epsilon^3)\,, \tag{2.13}$$

where the base-state area is

$$\mathscr{A}_0 = \int_0^\ell\int_{-1}^1 \mathscr{L}_0(\xi)\,\mathrm{d}\xi\,\mathrm{d}\eta = \ell\left(\frac{\sinh^{-1}k}{k} + \big(1+k^2\big)^{1/2}\right)\,, \tag{2.14}$$

the leading-order perturbation due to area changes within the surface is

$$\mathscr{A}_2^{(s)} = \int_0^\ell\int_{-1}^1 \mathscr{L}_2(\xi,\eta;\zeta)\,\mathrm{d}\xi\,\mathrm{d}\eta\,, \tag{2.15}$$

and the leading-order perturbation due to the curved walls causing a change in the domain for ξ is

$$\begin{aligned}\mathscr{A}_2^{(w)} &= -\frac{1}{\epsilon^2}\left[\int_0^\ell\int_{-1}^{-1+\frac{1}{2}\epsilon^2\zeta_-^2/(1+k^2)} \mathscr{L}_0(-1)\,\mathrm{d}\xi\,\mathrm{d}\eta \right.\\ &\qquad\left. + \int_0^\ell\int_{1-\frac{1}{2}\epsilon^2\zeta_+^2/(1+k^2)}^1 \mathscr{L}_0(1)\,\mathrm{d}\xi\,\mathrm{d}\eta\right]\,,\\ &= -\frac{1}{2}\int_0^\ell \big(1+k^2\big)^{-1/2}\left(\zeta_+^2+\zeta_-^2\right)\,\mathrm{d}\eta\,.\end{aligned} \tag{2.16}$$

2.3 *Euler–Lagrange equations for a minimal perturbed surface*

We now look for perturbed surfaces $\boldsymbol{x}(\xi,\eta)$ that minimize the area $\mathscr{A}$, relative to other nearby perturbations. This requirement means that the integral for $\mathscr{A}_2^{(s)}$ in (2.15) must be minimal with respect to variations in ζ. We impose this using the Euler–Lagrange equations:

$$\frac{\mathrm{d}}{\mathrm{d}\xi}\left(\frac{\partial\mathscr{L}_2}{\partial\zeta_\xi}\right)+\frac{\mathrm{d}}{\mathrm{d}\eta}\left(\frac{\partial\mathscr{L}_2}{\partial\zeta_\eta}\right)-\frac{\partial\mathscr{L}_2}{\partial\zeta}=0\,, \tag{2.17}$$

$$\Rightarrow\quad \frac{\partial}{\partial\xi}\left(\left(1+k^2\xi^2\right)^{1/2}\frac{\partial\zeta}{\partial\xi}\right)+\frac{\partial}{\partial\eta}\left(\left(1+k^2\xi^2\right)^{-1/2}\frac{\partial\zeta}{\partial\eta}\right) +2\left(1+k^2\xi^2\right)^{-3/2}k^2\zeta=0 \tag{2.18}$$

$$\Rightarrow\quad (1+k^2\xi^2)\frac{\partial^2\zeta}{\partial\xi^2}+\frac{\partial^2\zeta}{\partial\eta^2}+k^2\xi\frac{\partial\zeta}{\partial\xi}+\frac{2k^2\zeta}{1+k^2\xi^2}=0\,. \tag{2.19}$$

We now multiply equation (2.18) by ζ, and integrate over $\xi\in(-1,1)$, $\eta\in(0,\ell)$. Using integration by parts, we can relate the integral to that in (2.15), and hence show that

$$\mathscr{A}_2^{(s)}=\frac{1}{2}\int_0^\ell\left[\left(1+k^2\right)^{1/2}\zeta\frac{\partial\zeta}{\partial\xi}\right]_{\xi=-1}^{\xi=1}\mathrm{d}\eta\,. \tag{2.20}$$

The $O(\epsilon^2)$ change in area can then be written as

$$\mathscr{A}_2=\mathscr{A}_2^{(s)}+\mathscr{A}_2^{(w)}=\left[\int_0^\ell\left(1+k^2\right)^{1/2}\zeta\left(\frac{\partial\zeta}{\partial\xi}-\frac{\xi\zeta}{1+k^2}\right)\mathrm{d}\eta\right]_{\xi=-1}^{\xi=1}. \tag{2.21}$$

2.4 *Separation of variables*

We now express the solution for ζ of (2.19) in terms of axial Fourier modes, and decompose the radial functions into their even (symmetric) and odd (antisymmetric) components. Noting the boundary conditions (2.4), we therefore write

$$\zeta(\xi,\eta)=\sum_{n=1}^{\infty}\Big(a_n\,S_n(\xi)+b_n\,A_n(\xi)\Big)\,\sin\left(\frac{n\pi\eta}{\ell}\right), \tag{2.22}$$

where $S_n(\xi)=S_n(-\xi)$ are the symmetric parts, normalised by $S_n(0)=1$; and $A_n(\xi)=-A_n(-\xi)$ are the antisymmetric parts, normalised by $A_n'(0)=1$. The constants a_n and b_n are thus the values of the displacement and the radial displacement gradient of each axial Fourier mode at $\xi=0$.

Substituting (2.22) into (2.19), the different modes decouple, and each must satisfy

$$(1+k^2\xi^2)X''+k^2\xi X'+\left(\frac{2k^2}{1+k^2\xi^2}-\frac{n^2\pi^2}{\ell^2}\right)X=0\,, \tag{2.23}$$

where $X=S_n$ or $X=A_n$ as appropriate. Using the parity of the functions, we need only consider $\xi\in(0,1)$. Appropriate boundary conditions at $\xi=0$ are then

$$S_n(0)=1\,,\qquad S_n'(0)=0\,;\qquad A_n(0)=0\,,\qquad A_n'(0)=1\,. \tag{2.24a–d}$$

We now substitute (2.22) into (2.21) and perform the integration over η. The orthogonality of the Fourier modes means that only the diagonal terms in the double sums survive. The area change at $O(\epsilon^2)$ is then given by

$$\mathscr{A}_2 = \frac{\ell}{2}\left(1+k^2\right)^{1/2}\left\{\sum_{n=1}^{\infty} a_n^2\, S_n(1)\left(S_n'(1) - \frac{S_n(1)}{1+k^2}\right) + \sum_{n=1}^{\infty} b_n^2\, A_n(1)\left(A_n'(1) - \frac{A_n(1)}{1+k^2}\right)\right\}. \tag{2.25}$$

For a given helicity k, length ℓ, axial mode n, and parity, there will be a unique solution to (2.23) subject to (2.24), which is an area-minimising perturbation. The appropriate term in (2.25) gives the area change for the for that perturbation. Critical modes occur at certain values of k and ℓ when the area change is precisely zero. To find the critical lengths ℓ for each k, axial mode and parity, we therefore look for values of ℓ which allow us to solve equation (2.23) subject to the appropriate conditions from (2.24), together with either

$$X'(1) = \frac{X(1)}{1+k^2} \qquad \text{or} \qquad X(1) = 0\,, \tag{2.26a,b}$$

to give zero contribution to $\mathscr{A}_2$ in (2.25). This can be achieved numerically, either using a shooting algorithm, or with a finite-difference solver.

We note in passing that the condition (2.26a) is, to $O(\epsilon)$, equivalent to requiring that the perturbed surface meets the cylinder wall orthogonally. This can be seen by considering the scalar product of $(\partial\boldsymbol{x}/\partial\xi)\times(\partial\boldsymbol{x}/\partial\eta)$ (which is proportional to the normal to the surface) and the projection of $\boldsymbol{x}$ onto the x–y plane (which is proportional to the normal to the cylinder wall).

3. Finding the stability boundary

3.1 *Numerical results*

In equation (2.23), the mode number n can be absorbed into a single parameter $L = \ell/n$, so we need only find the critical values of L for each parity and each value of k.

For the even modes $S_n(\xi)$ a numerical shooting routine finds one critical value $L^*(k)$ of L for each $k \in [0,\infty)$ where condition (2.26a) can be satisfied. As $k \to 0$ we find $L^* \to 2.61$. As $k \to \infty$ we see $L^* \sim 3.14/k$. We also find a second critical value $L^0(k)$ for $k \in (1.51,\infty)$ where condition (2.26b) can be satisfied. As $k \to 1.51$ we find $L^0 \to \infty$. As $k \to \infty$ we again see $L^* \sim 3.14/k$. For $k < 1.51$ we were unable to find any values of L where where condition (2.26b) could be satisfied.

To avoid the divergence in these critical values of L as $k \to \infty$, we define $\Theta^* = kL^*(k)$ and $\Theta^0 = kL^0(k)$, and then plot Θ^* and Θ^0 against L in Fig. 3. The critical curves for the nth even mode are then given by $\theta = n\,\Theta^*(\ell/n)$ and $\theta = n\,\Theta^0(\ell/n)$. From (2.25), the $O(\epsilon^2)$ area change $\mathscr{A}_2$ is positive for $\theta < n\Theta^*(\ell/n)$ and for $\theta > n\Theta^0(\ell/n)$, and negative for $n\Theta^*(\ell/n) < \theta < n\Theta^0(\ell/n)$.[†]

For the odd modes $A_n(\xi)$, we are unable to find any finite values of L that give $\mathscr{A}_2 = 0$

[†] We adopt the convention when $\Theta^*(\ell)$ is not defined for a particular value of ℓ, we take $\Theta^* = -\infty$ to make sense of any inequalities.

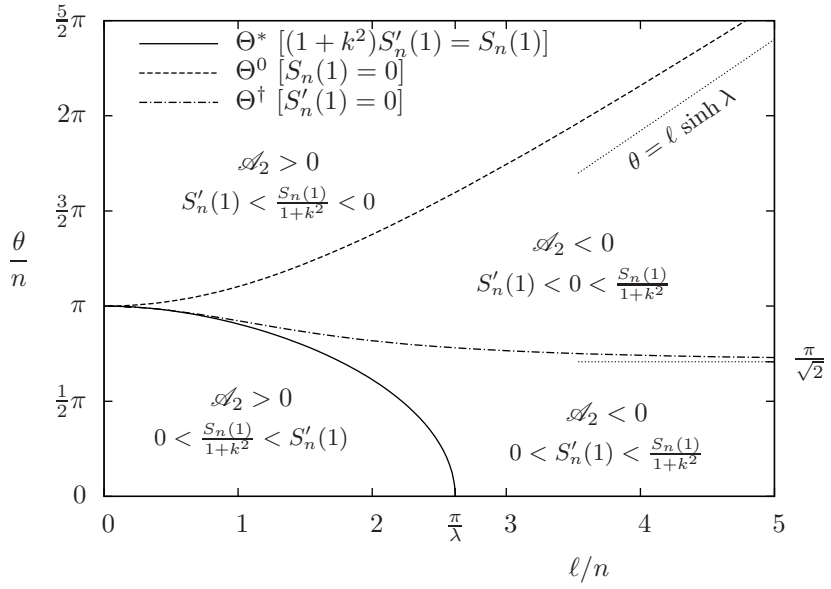

Fig. 3 The boundaries in θ–ℓ space dividing regions of different behaviour of the even modes $S_n(\xi)$ at $\xi = 1$. The three thick lines are obtained using a numerical shooting technique to solve the system (2.23)–(2.24b) for $X = S_n$, with either (2.26a), (2.26b) or (3.4a). The thin dotted lines are the asymptotic results as $\ell \to \infty$. $\lambda \approx 1.1997$ is the positive real root of $\lambda = \coth \lambda$.

for any k. Numerically solving the equation (2.23) for $A_n(\xi)$ subject to (2.24c) and (2.24d) at numerous points in (k, ℓ) parameter space suggests that $\mathscr{A}_2$ is always strictly positive, and certainly this would seem to be the case for $\theta < \Theta^*(\ell)$.

3.2 *Stability boundary*

We now argue that the curve $\theta = \Theta^*(\ell)$, as shown in Fig. 4, forms the stability boundary for the system. To accomplish this, we will show that the helicoid surface is stable for $\theta < \Theta^*(\ell)$, and unstable for $\theta > \Theta^*(\ell)$.

First suppose that $\Theta^*(\ell) < \theta < \Theta^0(\ell)$. Then the $n = 1$ even mode $S_0(\xi)$ corresponds to a deformation that yields a strictly smaller area at $O(\epsilon^2)$. Since there are no area changes at $O(\epsilon)$, this perturbation results in a decrease in surface area, and hence the original helicoid is unstable to this perturbation.

Now suppose $\theta \geq \Theta^0(\ell)$. We are still able to construct a deformation that results in a strictly smaller area, as follows. Consider the $n = 1$ even mode for the same value of $k = \ell/\theta$ but with smaller values ℓ' of ℓ and θ' of θ such that $\Theta^*(\ell') < \theta' < \Theta^0(\ell')$. (e.g. draw a straight line from the origin to the point (θ, ℓ) in Fig. 3, and then choose a point (θ', ℓ') on it that lies in the $\mathscr{A}_2 < 0$ region.) For $0 < \xi < \ell'$ we impose the deformation implied by this mode, while for $\ell' \leq \xi < \ell$ we impose zero deformation. The area change at $O(\epsilon^2)$ is simply the area change under the mode, which is negative. Hence the helicoid is unstable to this perturbation.

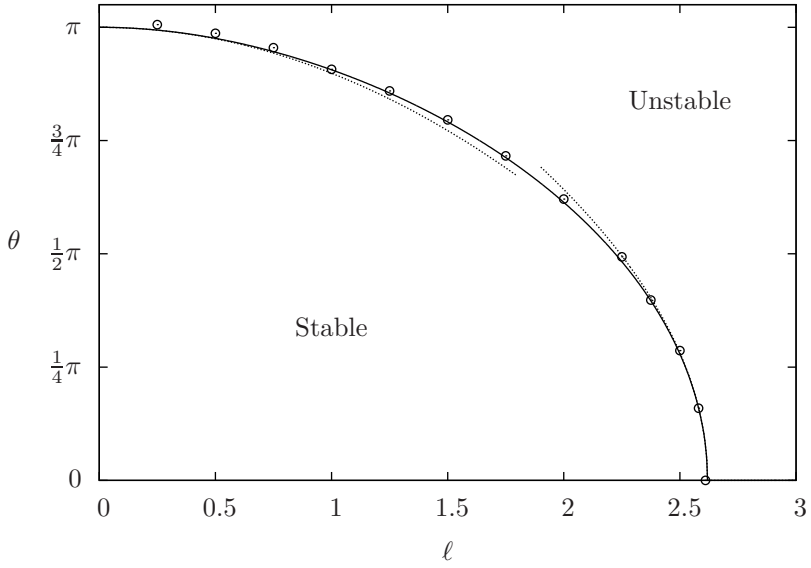

Fig. 4 The stability boundary $\theta = \Theta^*(\ell)$. Numerical results from the present work (continuous line) are shown alongside numerical simulations of the full surface (circles) as described in Appendix B. The dotted lines are the asymptotic solutions for large and small k, as described in §3.3.

Finally suppose that $\theta < \Theta^*$, which also implies $\theta < \Theta^0$. For any deformation $\zeta(\xi, \eta)$, we now construct a related deformation $\zeta^*(\xi, \eta)$ which satisfies (2.4) and has the same linearised contact line with the cylinder wall at $\xi = \pm 1$, but is a solution of (2.23). This is achieved by taking Fourier series of $\zeta(\pm 1, \eta)$ and using the Fourier coefficients to determine the coefficients a_n and b_n in (2.22). (This is possible, since $S_n(1)$ and $A_n(1)$ are always non-zero for $\theta < \Theta^0$.)

We show in Appendix A that for $\theta < \Theta^0$, solutions of (2.23) and (2.4) have the global minimal area for given Dirichlet boundary conditions at $\xi = \pm 1$. Hence the area of the ζ surface will be greater than or equal to that of the constructed ζ^* surface.

The net area change for ζ^* is given by (2.25) and is simply the sum of the changes for each individual mode. Since $\theta < \Theta^*$, all the modes give a strictly positive change, and hence net area change under ζ^* must be strictly positive. Thus, the area change under ζ must be strictly positive, and therefore the helicoid is stable to all perturbations.

The stability boundary was also obtained using numerical simulations conducted with the surface minimization software *Surface Evolver* (**5**). These simulations are a refined version of the results presented by Cox & Jones (**4**), and further details can be found in Appendix B. The simulation results are shown alongside the theoretical boundary $\theta = \Theta^*(\ell)$ in Fig. 4, and we see excellent agreement.

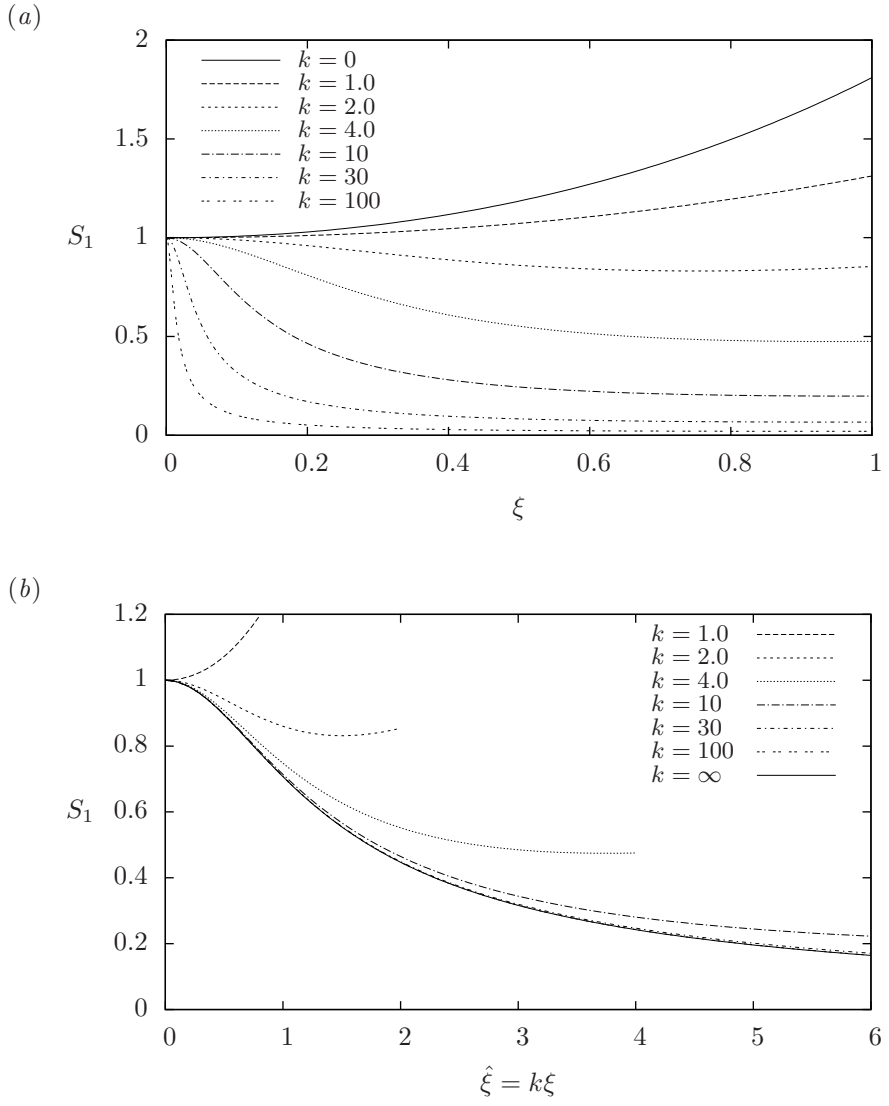

Fig. 5 The transverse functions $S_1(\xi)$ in the neutral perturbations $\zeta = \epsilon\, S_1(\xi)\, \sin(\pi\eta/\ell)$ at the stability boundary, for different values of k. The $k = 0$ and $k = \infty$ solutions are given analytically in (D.6) and (C.16). The other solutions are found numerically from the results in §3.1. Panel (b) shows the same curves with a rescaled horizontal axis, to demonstrate the self-similar form as $k \to \infty$.

3.3 *Limiting behaviour for small ℓ and θ*

The system (2.23)–(2.26a) for the even modes at the stability boundary can be analysed asymptotically in the limits $k \gg 1$ and $k \ll 1$, which correspond to small ℓ and small θ respectively. The detailed calculations can be found in Appendices C and D, where we obtain the following results for the stability boundary:

$$\theta \sim \pi \left(1 - \frac{\ell^2}{\pi^2}\right) \qquad \text{for} \qquad \ell \ll 1 \tag{3.1}$$

$$\theta \sim \sqrt{\frac{6\pi\lambda}{2+\lambda^2}} \left(\frac{\pi}{\lambda} - \ell\right)^{1/2} \qquad \text{for} \qquad \frac{\pi}{\lambda} - \ell \ll 1 \tag{3.2}$$

where $\lambda \approx 1.1997$ is the positive real root of $\lambda = \coth\lambda$. These two asymptotic limits are shown in Fig. 4 alongside the full numerical solutions and the simulations.

3.4 *Instability mechanisms*

The most unstable perturbations are given by the $n = 1$ even modes. The radial shapes $S_1(\xi)$ of these modes at the critical (neutral-stability) point for different values of k are shown in Fig. 5.

For small k (small θ) the instability mechanism is the obvious one, involving the contact lines with the cylinder wall moving away from the diameter to take advantage of the smaller distance across the cylinder. This loss of area at the wall ($\mathscr{A}_2^{(w)} < 0$) has to be balanced against the increase in area caused by the curvature in the axial direction ($\mathscr{A}_2^{(s)} > 0$). A critical length must be exceeded for the increase in $\mathscr{A}_2^{(s)}$ to be sufficiently small to be overcome by the decrease in $\mathscr{A}_2^{(w)}$. The form of the most unstable perturbation is qualitatively similar to the $k = 0$ solution, in which $\zeta = \epsilon \cosh(\lambda\xi)\sin(\pi\eta/\ell)$ (derived in Appendix D).

For larger k, however, a different mechanism applies. We can see from Fig. 5 that the critical modes for $k \gg 1$ are localised towards the centre of the cylinder at $\xi = 0$ and have negligible displacements at $\xi = 1$. The majority of the area reduction to offset the increases due to the axial profile therefore occurs due to the central displacements and not due to the displacement of the contact line at the boundary. The deformations around the centre-line allow an area saving on their own, without needing help from the external boundaries.

We can confirm that the area loss $\mathscr{A}_2^{(w)}$ caused by the movement of the contact point on the cylinder wall is unnecessary for instability, by removing that area-loss term from (2.21). The expression (2.25) for the $O(\epsilon^2)$ area change then becomes

$$\mathscr{A}_2 = \mathscr{A}_2^{(s)} = \frac{\ell}{2}\left(1+k^2\right)^{1/2} \sum_{n=1}^{\infty} \left\{ a_n^2\, S_n(1) S_n'(1) + A_n(1) A_n'(1) \right\}. \tag{3.3}$$

Hence, when solving (2.23) with (2.24), the appropriate boundary conditions to consider for each mode at $\xi = 1$ are

$$X_n'(1) = 0\,, \qquad \text{or} \qquad X_n(1) = 0\,, \tag{3.4a,b}$$

in place of (2.26).

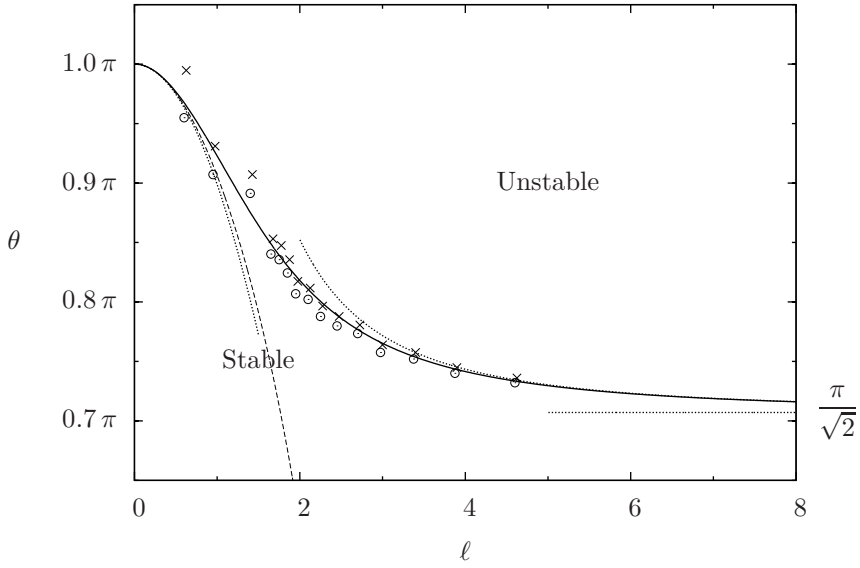

Fig. 6 The stability boundary for the case where there is no area saving from the cylindrical wall, i.e. the boundary condition (2.26a) is replaced by (3.4a). The theoretical boundary $\theta = \Theta^\dagger(\ell)$ is shown by the solid line. The dotted lines show the asymptotic results (C.29) and (E.15) for large and small k. Results from numerical simulations (see Appendix B) are also shown; circles representing configurations found to be stable, and crosses those found to be unstable. The thin dashed line shows the original stability boundary from Fig. 4.

Solving this new system numerically, we again only find solutions for the even modes. Solutions for the $S_n(1) = 0$ condition have already been obtained in §3.1. The new $S_n'(1) = 0$ condition results in a new boundary $\theta/n = \Theta^\dagger(\ell/n)$, which is shown in Fig. 3. The new stability boundary is shown in more detail in Fig. 6, along with asymptotic solutions for large and small k, and the results of numerical simulations (see below). The shape of the new neutrally stable $n = 1$ modes are shown in Fig. 7.

For $k \gg 1$, the asymptotic behaviour of the system is the same as for the previous case, as described in Appendix C. (Specifically, the leading-order and first-order corrections to θ in (C.29) are found to be independent of the area change at the outer wall.) The critical angle tends to $n\pi$ as $\ell \to 0$ as before, and the displacements in the critical modes become localised near $\xi = 0$.

For $k \ll 1$, the new calculations are presented in Appendix E. We find that the critical angle asymptotes to a constant $n\theta_\infty$ as $\ell \to \infty$, where $\theta_\infty = \pi/\sqrt{2}$. Therefore, with these boundary conditions, arbitrarily long helicoids are stable provided that the total twist θ is not greater than θ_∞. The radial functions $S_n(\xi)$ for the critical modes are almost uniform, but with a slightly larger displacement near $\xi = 0$ than towards $\xi = 1$.

As with the original problem, the stability boundary is also estimated using numerical simulations performed with *Surface Evolver*. The change in boundary conditions is equivalent to replacing the curved cylinder wall by a pair of walls generated by the normals

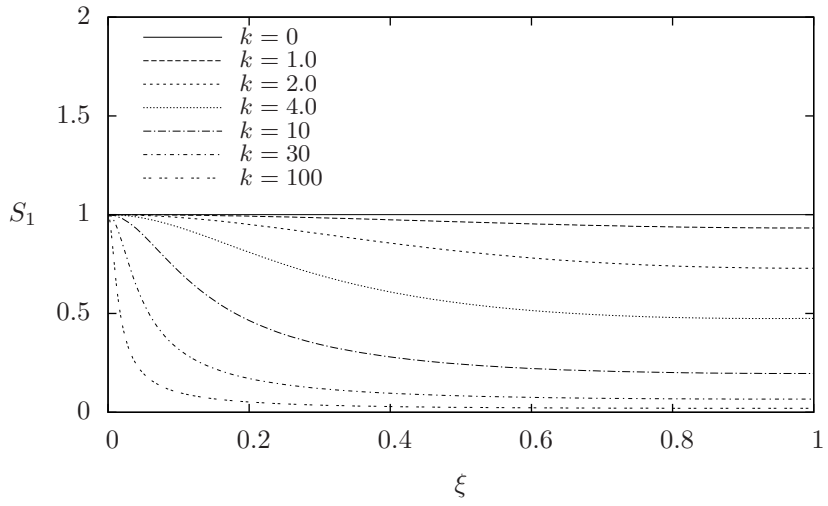

Fig. 7 The transverse functions $S_1(\xi)$ at the stability boundary, as in Fig. 5(a), but for the case where there is no area saving from the cylindrical wall. Different behaviour is seen for $k \leq O(1)$, but as $k \to \infty$, the solutions become asymptotically equal to those with the wall present; as shown in Fig. 5(a).

to the initial helicoid surface at $\xi = \pm 1$. Full details of the simulations are provided in Appendix B, and the results can be seen in Fig. 6.

This new system may actually be more relevant to the stability of films in a larger system, because it removes the external instability mechanism, namely the effect of the curved cylinder walls. From the form of the critical modes, we can see that the perturbations are localised along the centre-line, i.e. the most twisted part of the surface.

4. Stability with multiple vanes

Suppose that in the base state we now have N equally spaced helicoidal vanes emanating from a central singular line at $x = y = 0$, as depicted in Fig. 1(b). For $N = 3$, this is the standard configuration of a Plateau border. For $N = 2$ we return to the case of a single film as studied above.

Using the same dimensionless coordinate system as before, each vane is pinned to a cylinder radius at $z = 0$ and $z = \ell$, and the remaining edge lies on the cylinder wall $x^2 + y^2 = 1$ as before. At $z = 0$, the pinned radii lie at equally spaced angles $\theta_j = 2j\pi/N$, where $0 \leq j \leq N - 1$. At $z = \ell$, we have equally spaced angles $\theta + \theta_j$, so that each vane is subject to the same twist angle $\theta = k\ell$. The base-state location of the jth vane is thus given by

$$\boldsymbol{x}_0^{(j)}(\xi, \eta) = \begin{pmatrix} \xi \cos(\theta_j + k\eta) \\ \xi \sin(\theta_j + k\eta) \\ \eta \end{pmatrix} \tag{4.1}$$

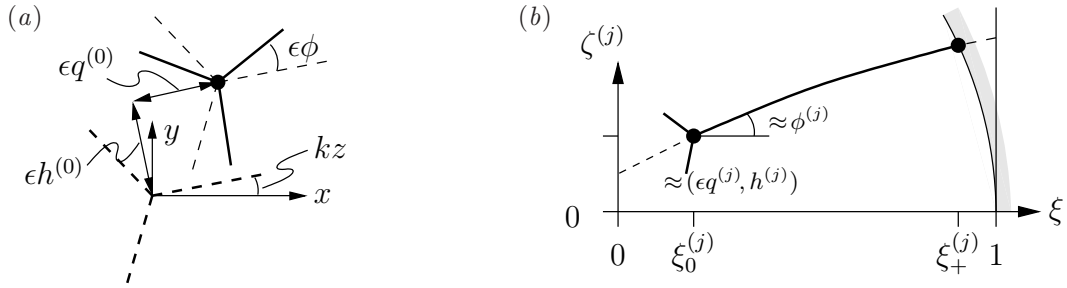

Fig. 8 The geometry of the film near the central singular line for the case of multiple vanes. (a) The central region at axial position z with $N = 3$ vanes. The singular line is originally at $x = y = 0$ with the the vanes shown by thick dashed lines. It is then displaced by $\epsilon(q^{(0)}, h^{(0)})$ and the vanes each rotated by an additional angle $\epsilon\phi$. The vanes in this displaced and rotated configuration are shown by thick solid lines. (b) The coordinates for describing the perturbation to the jth vane of the film, between the singular line at $\xi = \xi_0^{(j)}(\eta)$ and the cylinder wall at $\xi = \xi_+^{(j)}(\eta)$.

where $\eta \in (0, \ell)$ and $\xi \in (0, 1)$.

The perturbed position of the jth vane is then described by a function $\zeta^{(j)}(\xi, \eta)$ in the same way as in (2.3), namely

$$\boldsymbol{x}^{(j)}(\xi,\eta) = \begin{pmatrix} \xi\cos(\theta_j + k\eta) \\ \xi\sin(\theta_j + k\eta) \\ \eta \end{pmatrix} + \frac{\epsilon\,\zeta^{(j)}(\xi,\eta)}{(1+k^2\xi^2)^{1/2}} \begin{pmatrix} -\sin(\theta_j + k\eta) \\ \cos(\theta_j + k\eta) \\ -k\xi \end{pmatrix}. \tag{4.2}$$

The range of ξ is now restricted to $\xi \in (\xi_0^{(j)}(\eta), \xi_+^{(j)}(\eta))$, where $\xi_0^{(j)}$ is the point where the vane joins the (potentially displaced) singular line, and $\xi_+^{(j)}$ is (as before) the point where the vane meets the cylinder wall. See Fig. 8(b).

Suppose that under the perturbation (4.2), the central singular line at dimensionless axial position z is displaced in the x–y plane by $\epsilon q^{(0)}(z)$ and $\epsilon h^{(0)}(z)$ in the directions parallel and perpendicular to the unperturbed $j = 0$ vane. Suppose also that the vanes are rotated through an angle $\epsilon\phi(z)$ as they meet at the line. These perturbations are depicted in Fig. 8(a). (Note that the singular line may no longer lie parallel to the z axis, and that ϕ is measured in the plane perpendicular to the border.) All vanes are assumed to be rotated by the same angle $\epsilon\phi(z)$ at a given value of z. For if not, the angles that the surfaces meet at would not be equal, and we would be able to displace the border slightly to obtain a lower total surface area.

4.1 *Boundary conditions on* $\zeta^{(j)}$

We must now relate the functions $q^{(0)}(z)$, $h^{(0)}(z)$ and $\phi(z)$ that describe the displacement and rotation of the singular line, with the functions $\zeta^{(j)}(\xi, \eta)$ that describe the perturbation to each vane, in order to obtain boundary conditions on $\zeta^{(j)}$. But first we must define appropriate displacements and rotations relative to each vane.

Geometrically, the displacements $\epsilon q^{(j)}(z)$ and $\epsilon h^{(j)}(z)$ parallel and perpendicular to the

unperturbed jth vane are given in terms of those for the 0th vane by

$$q^{(j)}(z) = q^{(0)}(z)\,\cos\theta_j + h^{(0)}(z)\,\sin\theta_j\,, \tag{4.3}$$

$$h^{(j)}(z) = -q^{(0)}(z)\,\sin\theta_j + h^{(0)}(z)\,\cos\theta_j \tag{4.4}$$

Since the angle $\epsilon\phi$ is measured in the plane normal to the deformed singular line (rather than the x–y plane) we must also consider the rotation angles $\epsilon\phi^{(j)}(z)$ projected back to the x–y plane. The deformation of the singular line is by an $O(\epsilon)$ amount, and this leads to $O(\epsilon^2)$ changes in the projected angles. Hence

$$\phi^{(j)}(z) = \phi(z) + O(\epsilon)\,, \tag{4.5}$$

which is sufficient for our purposes.

At $\xi_0^{(j)}(\eta)$ (the point near $\xi = 0$ where the jth vane meets the singular line), the jth vane is perturbed axially by an amount

$$\delta^{(j)}(\eta) = \Big(\boldsymbol{x}^{(j)}(\xi_0^{(j)},\eta) - \boldsymbol{x}_0^{(j)}(\xi_0^{(j)},\eta)\Big)\cdot\begin{pmatrix}0\\0\\1\end{pmatrix} = -\frac{\epsilon\,k\,\xi_0^{(j)}\,\zeta^{(j)}(\xi_0^{(j)},\eta)}{\Big(1+k^2{\xi_0^{(j)}}^2\Big)^{1/2}}\,. \tag{4.6}$$

This means that points on the jth perturbed vane parameterised by η will meet the singular line at $z = \eta + \delta^{(j)}(\eta)$. Since we expect $\xi_0^{(j)} = O(\epsilon)$ and $\zeta^{(j)} = O(1)$, (4.6) implies that we will have $\delta^{(j)} = O(\epsilon^2)$.

For each j, we now equate the two expressions for the parallel displacement of the singular line at $z = \eta + \delta^{(j)}$; one from the vane displacement $\boldsymbol{x}^{(j)}$, and one from the singular-line displacement $q^{(j)}$. We obtain

$$\boldsymbol{x}^{(j)}\Big(\xi_0^{(j)},\eta\Big)\cdot\begin{pmatrix}\cos\big(\theta_j + k(\eta+\delta^{(j)})\big)\\ \sin\big(\theta_j + k(\eta+\delta^{(j)})\big)\\ 0\end{pmatrix} = \epsilon q^{(j)}(\eta+\delta^{(j)})\,. \tag{4.7}$$

Substituting from (4.2) and expanding in powers of ϵ, we find

$$\xi_0^{(j)} = \epsilon q^{(j)}(\eta) + O(\epsilon^3)\,. \tag{4.8}$$

Equating the equivalent pair of expressions for the perpendicular displacements of the singular line at $z = \eta + \delta^{(j)}$, we have

$$\boldsymbol{x}^{(j)}\Big(\xi_0^{(j)},\eta\Big)\cdot\begin{pmatrix}-\sin\big(\theta_j + k(\eta+\delta^{(j)})\big)\\ \cos\big(\theta_j + k(\eta+\delta^{(j)})\big)\\ 0\end{pmatrix} = \epsilon h^{(j)}(\eta+\delta^{(j)})\,. \tag{4.9}$$

Substituting from (4.2) and expanding in powers of ϵ, we find

$$\zeta^{(j)}(0,\eta) = h^{(j)}(\eta) + O(\epsilon)\,. \tag{4.10}$$

The condition on the rotation angle at $z = \eta + \delta^{(j)}$ is obtained by requiring that the normal to the perturbed vane makes the appropriate angle in the x–y plane, thus

$$\left(\frac{\partial\boldsymbol{x}^{(j)}}{\partial\xi}\Big(\xi_0^{(j)},\eta\Big)\times\frac{\partial\boldsymbol{x}^{(j)}}{\partial\eta}\Big(\xi_0^{(j)},\eta\Big)\right)\cdot\begin{pmatrix}\cos\big(\theta_j + kz + \epsilon\phi^{(j)}(z)\big)\\ \sin\big(\theta_j + kz + \epsilon\phi^{(j)}(z)\big)\\ 0\end{pmatrix} = 0\,. \tag{4.11}$$

Substituting from (4.2) and expanding in powers of ϵ, we find

$$\frac{\partial \zeta^{(j)}}{\partial \xi}(0,\eta) = \phi^{(j)}(\eta) + O(\epsilon) = \phi(\eta) + O(\epsilon)\,. \tag{4.12}$$

4.2 *Solution for the surface perturbations* $\zeta^{(j)}$

The condition for the perturbed vanes to be minimal is that each $\zeta^{(j)}$ satisfies the same equation (2.19) that we derived for the previous case. As before, we can construct solutions as the sum of orthogonal modes.

Noting that the functions $q^{(j)}$, $h^{(j)}$ and ϕ must vanish on $\eta = 0$ and $\eta = \ell$ (to satisfy the pinned boundary conditions), we represent them as Fourier series, thus

$$q^{(j)}(\eta) = \sum_{n=1}^{\infty} q_n^{(j)} \sin\left(\frac{n\pi\eta}{\ell}\right), \tag{4.13}$$

$$h^{(j)}(\eta) = \sum_{n=1}^{\infty} h_n^{(j)} \sin\left(\frac{n\pi\eta}{\ell}\right), \tag{4.14}$$

$$\phi(\eta) = \sum_{n=1}^{\infty} \phi_n \sin\left(\frac{n\pi\eta}{\ell}\right). \tag{4.15}$$

The solution to (2.19) subject to the boundary conditions (4.10) and (4.12) is then given by

$$\zeta^{(j)}(\xi,\eta) = \sum_{n=1}^{\infty} \left(h_n^{(j)} S_n(\xi) + \phi_n A_n(\xi)\right) \sin\left(\frac{n\pi\eta}{\ell}\right) + O(\epsilon) \tag{4.16}$$

where the S_n and A_n are as before, being solutions of (2.23) subject to (2.24).

4.3 *The area of the perturbed surfaces*

In a manner analogous to (2.6), we define the surface area per unit coordinate area for the perturbed jth vane by

$$\mathscr{L}^{(j)} = \left|\frac{\partial \boldsymbol{x}^{(j)}}{\partial \xi} \times \frac{\partial \boldsymbol{x}^{(j)}}{\partial \eta}\right|, \tag{4.17}$$

and expand it in powers of ϵ by writing $\mathscr{L}^{(j)} = \mathscr{L}_0^{(j)} + \epsilon^2 \mathscr{L}_2^{(j)} + O(\epsilon^3)$ as in (2.10)–(2.12). (As before there is no $O(\epsilon)$ term because the original helicoidal surfaces are extremal.)

The area of the perturbed surface of the jth vane is then given by

$$\mathscr{A}^{(j)} = \int_0^{\ell}\int_{\xi_0^{(j)}}^{\xi_+^{(j)}} \mathscr{L}^{(j)}(\xi,\eta;\zeta^{(j)})\,\mathrm{d}\xi\,\mathrm{d}\eta = \mathscr{A}_0^{(j)} + \epsilon\mathscr{A}_1^{(j)} + \epsilon^2\mathscr{A}_2^{(j)} + O(\epsilon^3)\,. \tag{4.18}$$

The leading-order term in the expansion is

$$\mathscr{A}_0^{(j)} = \int_0^{\ell}\int_0^{1} \mathscr{L}_0^{(j)}(\xi)\,\mathrm{d}\xi\,\mathrm{d}\eta = \frac{\ell}{2}\left(\frac{\sinh^{-1} k}{k} + \left(1+k^2\right)^{1/2}\right), \tag{4.19}$$

which gives the base-state area, as before. The first-order term is

$$\mathscr{A}_1^{(j)} = \frac{1}{\epsilon}\int_0^{\ell}\int_0^{\epsilon q^{(j)}} \mathscr{L}_0^{(j)}(0,\eta;\zeta^{(j)})\,\mathrm{d}\xi\,\mathrm{d}\eta = \int_0^{\ell} q^{(j)}(\eta)\,\mathrm{d}\eta\,, \tag{4.20}$$

which gives the correction due to the displacement of the central singular line. The second-order term is

$$\begin{aligned}\mathscr{A}_2^{(j)} &= \int_0^{\ell}\int_0^{1} \mathscr{L}_2^{(j)}(\xi,\eta;\zeta^{(j)})\,\mathrm{d}\xi\,\mathrm{d}\eta - \frac{1}{\epsilon^2}\int_0^{\ell}\int_{1-\frac{1}{2}\epsilon^2{\zeta_+^{(j)}}^2/(1+k^2)}^{1} \mathscr{L}_0^{(j)}(1,\eta;\zeta^{(j)})\,\mathrm{d}\xi\,\mathrm{d}\eta\,,\\ &= \frac{1}{2}\int_0^{\ell}\left[\left(1+k^2\right)^{1/2}\zeta^{(j)}\frac{\partial\zeta^{(j)}}{\partial\xi}\right]_0^1\mathrm{d}\eta - \frac{1}{2}\int_0^{\ell}\left(1+k^2\right)^{-1/2}{\zeta_+^{(j)}}^2\,\mathrm{d}\eta\,,\\ &= \frac{1}{2}\int_0^{\ell}\left(1+k^2\right)^{1/2}\left(\zeta_+^{(j)}\left.\frac{\partial\zeta^{(j)}}{\partial\xi}\right|_{\xi=1} - h^{(j)}\phi - \frac{{\zeta_+^{(j)}}^2}{1+k^2}\right)\mathrm{d}\eta\,,\end{aligned} \tag{4.21}$$

which gives the combined effect of changes within the surface and changes due to the movement of the contact line with the outer wall.

We now substitute the series expansions (4.13)–(4.16) into the area expressions (4.19)–(4.21). We then sum over the N vanes, and perform the integration over η. For future use, we note the results that

$$\sum_{j=0}^{N-1} h_n^{(j)} = 0\,, \qquad \sum_{j=0}^{N-1} q_n^{(j)} = 0\,, \tag{4.22a,b}$$

which are derived in Appendix F.

From (4.19), the total base-state area is simply

$$\mathscr{A}_0 = \sum_{j=0}^{N-1}\mathscr{A}_0^{(j)} = \frac{N\ell}{2}\left(\frac{\sinh^{-1}k}{k} + \left(1+k^2\right)^{1/2}\right). \tag{4.23}$$

From (4.20), the total $O(\epsilon)$ area change is

$$\mathscr{A}_1 = \sum_{j=0}^{N-1}\mathscr{A}_1^{(j)} = \sum_{n=1}^{\infty}\sum_{j=0}^{N-1} q_n^{(j)}\Big(1-(-1)^n\Big)\frac{\ell}{n\pi} = 0\,, \tag{4.24}$$

owing to the vanishing sum (4.22b) of the $q_n^{(j)}$'s over j.

From (4.21), the total $O(\epsilon^2)$ area change becomes

$$\begin{aligned}\mathscr{A}_2 = \sum_{j=0}^{N-1}\mathscr{A}_2^{(j)} = \frac{\ell}{4}(1+k^2)^{1/2}\sum_{n=1}^{\infty}\Bigg[&H^2 S_n(1)\left(S_n'(1) - \frac{S_n(1)}{1+k^2}\right)\\ &+ N\phi_n^2 A_n(1)\left(A_n'(1) - \frac{A_n(1)}{1+k^2}\right)\Bigg]\,,\end{aligned} \tag{4.25}$$

where we have used (4.22a) and defined

$$H^2 = \sum_{j=0}^{N-1}{h_n^{(j)}}^2 = \begin{cases} 2{h_n^{(0)}}^2 & : \quad N=2\\ \frac{1}{2}N\left({h_n^{(0)}}^2 + {q_n^{(0)}}^2\right) & : \quad N\geq 3\end{cases} \tag{4.26}$$

as derived in Appendix F. (As before, only the diagonal terms survive the integration owning to the orthogonality of the axial Fourier modes.)

We have already seen in §3.1 that the quantity multiplying ϕ_n^2 is always positive. So the critical case of $\mathscr{A}_2 = 0$ is first achieved for each Fourier mode when $\phi_n = 0$ and

$$S_n'(1) = \frac{S_n(1)}{1+k^2} \qquad \text{or} \qquad S_n(1) = 0\,. \tag{4.27a,b}$$

These conditions are independent of N, and are the same as for the single-film case studied above. Hence the multiple-vane system has the same stability boundary as the original system.

5. Conclusions

In this paper, we have presented a mathematical theory to describe the surface-tension-driven stability of helicoidal surfaces inside a circular cylinder, as shown in Fig. 1. The key parameters are the aspect ratio ℓ (height H divided by radius R) and the total twist angle θ between the two ends.

The method we use in §2 and §3 is to find the most unstable perturbation to the surface and then to look for the critical cases in which this perturbation results in no change to the overall surface area. By using separation of variables, the problem is reduced to solving a one-dimensional second-order ODE in the radial coordinate, which can be carried out numerically. Our results for the stability boundary in θ–ℓ space are in good agreement with those obtained previously by Cox & Jones (**4**) via full numerical simulations (Fig. 4).

Asymptotic expansions of the stability boundary and the critical perturbation surfaces have also been obtained for large and small pitch parameters $k = \theta/\ell$. These show that two different instability mechanisms operate as the total twist θ varies. For small and moderate θ, the obvious mechanism of normal displacements that save area due to the converging cylindrical walls operates. But for larger θ, internal perturbations to the surface are sufficient, even in the absence of any savings from the cylinder walls.

This second mechanism is confirmed by computing the stability boundary for perturbations where there is no area saving from the walls (Fig. 6). The critical angle is close to the previous case for $\ell \ll 1$, but behaves differently as ℓ increases, varying monotonically between $\theta = \pi$ as $\ell \to 0$ and $\theta = \pi/\sqrt{2}$ as $\ell \to \infty$.

We also consider the case of multiple vanes, arranged symmetrically about a central axis, as studied by Cox & Jones (**4**) (Fig. 1*b*). Their numerical and experimental results suggested that the stability boundary was the same as (or at least very close to) that of the single vane case. In §4, we have proved mathematically that the stability problem for the multiple-vane case is equivalent to the single-vane case, and hence the stability boundaries are identical. Physically this is due to the fact that $O(\epsilon)$ changes in area due to the displacement of the central singular line (a Plateau border for the case $N = 3$) all cancel out to sufficiently high accuracy. The overall area changes are still dominated by deformations in the film surfaces and the moving contact line with the cylinder walls, which are described by the same equations.

The stability boundary for the case of no wall area saving is likely to be more relevant to the case of Plateau borders in foams (the original motivation for the work of Cox & Jones (**4**)) as there will be no such savings as each surface from the Plateau border in question

joins other Plateau borders elsewhere in the form. The effect of the neighbouring borders should act to increase the stability as they provide an anchoring effect. Applying the no-wall-area-saving boundary to the three-vane problem suggests that Plateau borders will always be stable for total twists $\theta \leq \pi/\sqrt{2}$. Above this limit, it will depend on the length of the border (longer borders being more unstable) and the detailed interactions with the neighbouring borders. But internal instabilities are at least possible for $\theta > \pi/\sqrt{2}$.

Acknowledgements

SC acknowledges financial support from the FP7 IAPP project HYDROFRAC (PIAP-GA-2009-251475), and also thanks K. Brakke for assistance with the *Surface Evolver* software.

References

1. J. A. F. Plateau, *Statique Expérimentale et Théorique des Liquides soumis aux Seules Forces Moléculaires*. Gauthier–Villars, Paris (1873).

2. J. E. Taylor, The structure of singularities in soap-bubble-like and soap-film-like minimal surfaces. *Anal. Math.* **103** (1967) 489–539.

3. D. Weaire, M. F. Vaz, P. I. C. Teixeira and M. A. Fortes, Instabilities in liquid foams. *Soft Matter* **3** (2007) 47–57.

4. S. J. Cox and S. A. Jones, Instability of stretched and twisted soap films in a cylinder. *J. Engr Math.* **86** (2014) 1–7.

5. K. Brakke, The Surface Evolver. *Expt Math.* **1** (1992) 141–165.

APPENDIX A

Proof that solutions to (2.19) have minimal area for $\theta < \Theta^0$

In this appendix, we prove that when $\theta < \Theta^0(\ell)$, perturbations that satisfy (2.19) and (2.4) attain the minimum surface area at $O(\epsilon^2)$ of any perturbation that satisfies the same Dirichlet boundary conditions at $\xi = \pm 1$ and $\eta = 0, \ell$. This result is used in the proof of the stability boundary in §3.2.

Let $\zeta^*(\xi, \eta)$ be a perturbation that satisfies the pinned diameter conditions (2.4) and the field equation (2.19). Now consider a general perturbation $\zeta(\xi, \eta)$ which satisfies (2.4) and has $\zeta(\pm 1, \eta) = \zeta^*(\pm 1, \eta)$. We now define $\zeta'(\xi, \eta)$ by writing

$$\zeta(\xi, \eta) = \zeta^*(\xi, \eta) + \delta\, \zeta'(\xi, \eta)\,, \tag{A.1}$$

where $\delta > 0$ is an arbitrary scale. We therefore have $\zeta'(\xi, 0) = \zeta'(\xi, \ell) = 0$ and $\zeta'(\pm 1, \eta) = 0$. We now consider the $O(\epsilon^2)$ area change $\mathscr{A}_2 \equiv \mathscr{A}_2^{(w)} + \mathscr{A}_2^{(s)}$ under the general perturbation ζ, and relate it to the same change under ζ^*.

The area change $\mathscr{A}_2^{(w)}$ is defined in (2.16). With the boundary conditions $\zeta_\pm \equiv \zeta(\pm 1, \eta)$ fixed, $\mathscr{A}_2^{(w)}$ for the ζ surface is constant, and equal to that for the ζ^* surface. We therefore need only consider $\mathscr{A}_2^{(s)}$, as defined in (2.15), where $\mathscr{L}_2$ is given by (2.21). Expanding ζ using (A.1) we find that

$$\mathscr{A}_2^{(s)} = \int_0^\ell \int_{-1}^1 \mathscr{L}_2(\xi, \eta; \zeta)\, \mathrm{d}\xi\, \mathrm{d}\eta = I_0 + \delta I_1 + \delta^2 I_2\,, \tag{A.2}$$

where

$$I_0 = \int_0^\ell \int_{-1}^1 \mathscr{L}_2(\xi, \eta; \zeta^*)\, \mathrm{d}\xi\, \mathrm{d}\eta\,, \tag{A.3}$$

$$\begin{aligned} I_1 &= \int_0^\ell \int_{-1}^1 \left[\frac{\partial \zeta'}{\partial \xi} \frac{\partial \mathscr{L}_2}{\partial \zeta_\xi} + \frac{\partial \zeta'}{\partial \eta} \frac{\partial \mathscr{L}_2}{\partial \zeta_\eta} + \zeta' \frac{\partial \mathscr{L}_2}{\partial \zeta} \right]_{\zeta=\zeta^*} \mathrm{d}\xi\, \mathrm{d}\eta\,, \\ &= \int_0^\ell \int_{-1}^1 \zeta' \left[-\frac{\mathrm{d}}{\mathrm{d}\xi} \left(\frac{\partial \mathscr{L}_2}{\partial \zeta_\xi} \right) - \frac{\mathrm{d}}{\mathrm{d}\eta} \left(\frac{\partial \mathscr{L}_2}{\partial \zeta_\eta} \right) + \frac{\partial \mathscr{L}_2}{\partial \zeta} \right]_{\zeta=\zeta^*} \mathrm{d}\xi\, \mathrm{d}\eta\,, \end{aligned} \tag{A.4}$$

(using integration by parts), and

$$\begin{aligned} I_2 &= \frac{1}{2} \int_0^\ell \int_{-1}^1 \left[\left(\frac{\partial \zeta'}{\partial \xi} \right)^2 \frac{\partial^2 \mathscr{L}_2}{\partial \zeta_\xi^2} + \left(\frac{\partial \zeta'}{\partial \eta} \right)^2 \frac{\partial^2 \mathscr{L}_2}{\partial \zeta_\eta^2} + \zeta'^2 \frac{\partial^2 \mathscr{L}_2}{\partial \zeta^2} \right]_{\zeta=\zeta^*} \mathrm{d}\xi\, \mathrm{d}\eta\,, \\ &= \int_0^\ell \int_{-1}^1 \mathscr{L}_2(\xi, \eta; \zeta')\, \mathrm{d}\xi\, \mathrm{d}\eta\,. \end{aligned} \tag{A.5}$$

The first integral I_0 is simply the value of $\mathscr{A}_2^{(s)}$ under the perturbation ζ^*. The second integral I_1 vanishes because ζ^* satisfies the Euler–Lagrange equation (2.17) as it is equivalent to (2.19). The difference in area between the ζ and ζ^* surfaces is therefore controlled entirely by the third integral I_2. This is seen to be equal to the $O(\epsilon^2)$ area change under ζ', where ζ' is regarded as a direct perturbation from the base state.

For ζ^* to attain the minimum area over all surfaces ζ satisfying $\zeta(\pm 1, \eta) = \zeta^*(\pm 1, \eta)$, we must show that I_2 is always positive for any ζ' satisfying $\zeta'(\pm 1, \eta) = 0$. This is certainly the case at $\theta = 0$, for then we are dealing with perturbations to a rectangular planar surface with all four edges fixed.

Now consider the region of θ–ℓ space where this continues to hold. On the boundary of this region, we must have a deformation ζ' which has zero area change, and no deformations with a strictly negative area change. Hence the ζ' which has zero area change must be minimal, and therefore must satisfy (2.19). We have already seen above that the only solutions of (2.19) with $\zeta(\pm 1, \eta) = 0$ are composed of symmetric modes that lie on the lines $\theta = n\Theta^0(\ell/n)$.

Continuing upwards from $\theta = 0$, we see from Fig. 3 that the first boundary we meet is the $n = 1$ curve $\theta = \Theta^0(\ell)$. Thus for $\theta < \Theta^0(\ell)$, all perturbations ζ' satisfying $\zeta'(\pm 1, \eta) = 0$ result in positive area changes. Hence within this region I_2 is positive, and the solution ζ^* has the minimal area.

APPENDIX B

Numerical Simulations

The numerical simulations of the stability of a single film inside a cylinder, shown in Fig. 4, were performed using *Surface Evolver* (**5**). Following Cox & Jones (**4**), the two ends of the surface are fixed on diameters at $z = 0$ and $z = \ell$ with relative twist $\theta = k\ell$, and the two sides are constrained to move on a cylinder $x^2 + y^2 = 1$. Minimizing the area of the film causes the film to meet the curved cylinder wall normally when a stable configuration exists. The stability boundary was found by fixing ℓ and gradually increasing θ from zero in small steps, minimizing area at each step, until the lowest eigenvalue of the Hessian became negative, indicating instability.

The data shown in Fig. 4 were generated with a higher level of refinement (more triangles representing the surface) and smaller steps in twist angle between each minimization than in (**4**), evident in the better agreement with the theory at low ℓ.

To simulate the case of a single film without the area saving from the curved cylindrical wall, the constraint of contact with the cylindrical wall must be replaced by a constraint of contact with

a new wall. The shape of this will must ensure that there is no area losses or gains at the edge when the film is displaced from its initial helicoidal configuration. Such a wall must therefore be normal to the initial helicoidal surface at its edges. See Fig. 2.

The two walls (one for each edge of the initial helicoid) can be described parametrically, with the equations deduced from (2.3). We take $\xi = \pm 1$ to place us on the two edges of the initial helicoid, and (without loss of generality) we set $\epsilon = 1$. Then varying η and ζ moves $\boldsymbol{x}$ along the edge and normal to the helicoid respectively. Hence the walls are given parametrically by

$$x(\eta,\zeta) = \pm\cos(k\eta) - \frac{\zeta\sin(k\eta)}{(1+k^2)^{1/2}} \tag{B.1}$$

$$y(\eta,\zeta) = \pm\sin(k\eta) + \frac{\zeta\cos(k\eta)}{(1+k^2)^{1/2}} \tag{B.2}$$

$$z(\eta,\zeta) = \eta \mp \frac{k\zeta}{(1+k^2)^{1/2}}. \tag{B.3}$$

For computational efficiency, the wall surfaces are each written as a one-parameter family of curves, with η parameterizing the family member and ζ parameterizing the position along each curve. Each edge vertex of the surface tessellation is then constrained to move on one curve from the family, i.e. with its value of η fixed.

The shape of the boundary walls now depends on the parameter $k = \theta/\ell$, so if θ is varied while ℓ is held fixed, the shape will change. When determining the stability boundary, it was therefore more convenient to fix k and vary ℓ, with $\theta = k\ell$ varying accordingly. The simulation results for this case are shown in Fig. 6.

APPENDIX C

Asymptotic solution for $k \gg 1$

As $k \to \infty$, our numerical results for the stability boundary (see §3.1) suggest that $\ell \to 0$ and θ tends to a finite limit, close to π. We verify that these limits are exact by calculating an asymptotic solution for $k \gg 1$.

For $\xi = O(1)$ in the ODE (2.23), the dominant terms as $k \to \infty$ are $O(k^2)$, which suggests we would need to take $\ell = O(k^{-1})$ to retain any ℓ-dependence in the equation. There is also another distinguished length scale, namely $\xi = O(k^{-1})$. On this scale, the dominant terms are again $O(k^2)$, and we need to take $\ell = O(k^{-1})$ to retain the ℓ-dependence.

We now consider a matched asymptotic expansion for $k \gg 1$. We guess that the limiting value of the critical θ is $n\pi$, and thus write

$$\ell = \frac{\theta}{k} = \frac{n\pi}{k}\Big(1 + \alpha k^{-2} + \ldots\Big), \tag{C.1}$$

for some constant α. We now consider separate solutions to (2.23) for $\xi = O(1)$ and $\xi = O(k^{-1})$.

C.1 *Outer solution for $\xi = O(1)$*

The governing equation (2.23) can be written as

$$(\xi^2 + k^{-2})X'' + \xi X' + 2k^{-2}(\xi^2 + k^{-2})^{-1}X - (1 + \alpha k^{-2} + \ldots)^{-2}X = 0\,, \tag{C.2}$$

and, from (2.26a), we have the outer boundary condition

$$X'(1) = k^{-2}(1 + k^{-2})^{-1}X(1)\,. \tag{C.3}$$

We then write

$$X(\xi) = \frac{1}{k}\Big(X_1(\xi) + k^{-2}X_3(\xi) + \ldots\Big) \tag{C.4}$$

(The initial factor of k^{-1} is to aid matching with the $O(1)$ inner solution for X, which, as we shall see below, decays like $(k\xi)^{-1}$ as $\xi \to \infty$.)

At $O(k^{-1})$, (C.2) and (C.3) become

$$\xi^2 X_1'' + \xi X_1' - X_1 = 0\,, \qquad X_1'(1) = 0\,. \tag{C.5a,b}$$

Since the equation is linear and homogeneous in ξ, we look for solutions that are the sum of terms proportional to powers of ξ. The particular solution that satisfies the equation and boundary condition (C.5) is found to be

$$X_1 = A\left(\frac{1}{\xi} + \xi\right)\,, \tag{C.6}$$

where A is an unknown constant that will be determined later by matching.

At $O(k^{-3})$ we have

$$\begin{aligned}\xi^2 X_3'' + \xi X_3' - X_3 &= -\Big[X_1'' + 2\xi^{-2}X_1 + 2\alpha X_1\Big] \\ &= -4A\xi^{-3} - 2A(1+\alpha)\xi^{-1} - 2\alpha A\xi\,,\end{aligned} \tag{C.7}$$

subject to

$$X_3'(1) = X_1(1) \quad \Rightarrow \quad X_3'(1) = 2A\,. \tag{C.8}$$

Since $\xi^{\pm 1}$ are solutions of the homogeneous equation, we seek a solution of the form

$$X_3(\xi) = \Big(C\xi^{-1} + D\xi\Big) + \Big(E\xi^{-3} + F\xi^{-1}\log\xi + G\xi\log\xi\Big)\,. \tag{C.9}$$

The constants E, F, and G are found by insisting the solution satisfies (C.7), while the boundary condition (C.8) gives a relationship between C and D. We find

$$X_3(\xi) = C\left(\xi^{-1} + \xi\right) - \tfrac{1}{2}A\xi^{-3} + (1+\alpha)A\xi^{-1}\log\xi - \alpha A\xi\log\xi - \tfrac{1}{2}A\xi\,. \tag{C.10}$$

The remaining constant C will be determined by matching with the inner solution.

C.2 *Inner solution for $\xi = O(k^{-1})$*

We write $\xi = k^{-1}\hat{\xi}$ and $X(\xi) = \hat{X}(\hat{\xi})$. The governing equation (2.23) then becomes

$$(1+\hat{\xi}^2)\hat{X}'' + \hat{\xi}\hat{X}_n' + \left(\frac{2}{1+\hat{\xi}^2} - (1 + \alpha k^{-2} + \ldots)^{-2}\right)\hat{X} = 0\,. \tag{C.11}$$

From (2.24a) and (2.24b), the boundary conditions at $\hat{\xi} = 0$ are

$$\hat{X}(0) = 1\,, \qquad \hat{X}'(0) = 0\,. \tag{C.12a,b}$$

We then write

$$\hat{X}(\hat{\xi}) = \hat{X}_0(\hat{\xi}) + k^{-2}\hat{X}_2(\hat{\xi}) + \ldots\,. \tag{C.13}$$

At $O(1)$ in k, (C.11) and (C.12) become

$$(1+\hat{\xi}^2)\hat{X}_0'' + \hat{\xi}\hat{X}_0' + \left(\frac{2}{1+\hat{\xi}^2} - 1\right)\hat{X}_0 = 0\,, \tag{C.14}$$

subject to

$$\hat{X}_0(0) = 1\,, \qquad \hat{X}_0'(0) = 0\,. \tag{C.15a,b}$$

We notice that this system has an exact solution

$$\hat{X}_0(\hat{\xi}) = \left(1+\hat{\xi}^2\right)^{-1/2} . \tag{C.16}$$

Since we have a second-order equation with two independent boundary conditions, this solution is unique. The fact that this solution decays as $\hat{\xi} \to \infty$ (which enables matching with the outer solution) validates our choice of leading-order constant in the expansion (C.1).

At $O(k^{-2})$, (C.11) and (C.12) become

$$\begin{aligned}(1+\hat{\xi}^2)\hat{X}_2'' + \hat{\xi}\hat{X}_2' + \left(\frac{2}{1+\hat{\xi}^2} - 1\right)\hat{X}_2 &= -2\alpha_2\hat{X}_0\,, \\ &= -\frac{2\alpha}{(1+\hat{\xi}^2)^{1/2}}\end{aligned} \tag{C.17}$$

subject to

$$\hat{X}_2(0) = 0\,, \qquad \hat{X}_2'(0) = 0\,. \tag{C.18}$$

We can make progress here by writing

$$\hat{X}_2(\hat{\xi}) = \left(1+\hat{\xi}^2\right)^{-1/2} f(\hat{\xi}) \tag{C.19}$$

Substituting (C.19) into (C.17), the equation for $f(\hat{\xi})$ is then

$$f'' - \frac{\hat{\xi}}{1+\hat{\xi}^2} f' = -\frac{2\alpha}{1+\hat{\xi}^2} \tag{C.20}$$

subject to $f(0) = f'(0) = 0$. An integrating factor can be employed to transform the equation to

$$\frac{\mathrm{d}}{\mathrm{d}\hat{\xi}}\left[\frac{1}{(1+\hat{\xi}^2)^{1/2}} f'(\hat{\xi})\right] = -\frac{2\alpha}{(1+\hat{\xi}^2)^{3/2}}\,, \tag{C.21}$$

and thence

$$f'(\hat{\xi}) = -2\alpha(1+\hat{\xi}^2)^{1/2}\int_0^{\hat{\xi}} \frac{1}{(1+t^2)^{3/2}}\,\mathrm{d}t = -2\alpha(1+\hat{\xi}^2)^{1/2}\left[\frac{t}{(1+t^2)^{1/2}}\right]_0^{\hat{\xi}} = -2\alpha\hat{\xi}\,, \tag{C.22}$$

where we applied the boundary condition $f'(0) = 0$ to arrive at the definite integral. Integrating once more, and applying the condition $f(0) = 0$, we obtain

$$f(\hat{\xi}) = -\alpha\hat{\xi}^2\,. \tag{C.23}$$

Hence

$$\hat{X}_2(\hat{\xi}) = -\frac{\alpha\hat{\xi}^2}{\left(1+\hat{\xi}^2\right)^{1/2}}\,. \tag{C.24}$$

C.3 *Matching at intermediate ξ*

We introduce an intermediate variable $x = k^{-1/2}\hat{\xi} = k^{1/2}\xi$, and consider the expansion of both the inner and outer solutions at $x = O(1)$. The outer solution (C.4) is asymptotically

$$X \sim k^{-1/2}\left(\frac{A}{x}\right) + k^{-3/2}\left(Ax - \frac{A}{2x^3}\right) + O(k^{-5/2})\,, \tag{C.25}$$

while the inner solution (C.13) is

$$\begin{aligned}\hat{X} &\sim \hat{\xi}^{-1}\left(1+\hat{\xi}^{-2}\right)^{-1/2} - \alpha k^{-2}\hat{\xi}\left(1+\hat{\xi}^{-2}\right)^{-1/2} + \dots \\ &\sim k^{-1/2}\left(\frac{1}{x}\right) + k^{-3/2}\left(-\frac{1}{2x^3} - \alpha x\right) + O(k^{-5/2})\,. \end{aligned} \tag{C.26}$$

Matching at $O(k^{-1/2})$ we must take $A = 1$, and matching at $O(k^{-3/2})$ we find $\alpha = -1$. (The constant C would be found by matching at $O(k^{-5/2})$, but it is not needed for our purposes.)

C.4 *Asymptotic expression for $\theta(\ell)$*

Putting $\alpha = -1$ in (C.1) we have

$$\theta = n\pi\Big(1 - k^{-2} + O(k^{-4})\Big)\,. \tag{C.27}$$

Now

$$k = \frac{\theta}{\ell} = \frac{n\pi}{\ell}\Big(1 + O(k^{-2})\Big) = \frac{n\pi}{\ell}\Big(1 + O(\ell^2)\Big)\,, \tag{C.28}$$

and so we obtain

$$\theta = n\pi\Big(1 - \frac{\ell^2}{n^2\pi^2} + O(\ell^4)\Big)\,. \tag{C.29}$$

APPENDIX D

Asymptotic solution for $k \ll 1$

As $k \to 0$, the numerical results for the stability boundary suggest that $L = \ell/n$ tends to a constant, with an $O(k^2)$ residual. We therefore assume expansions of the form

$$X(\xi) = X_0(\xi) + k^2 X_2(\xi) + k^4 X_4(\xi) + \dots\,, \qquad \ell = \frac{n\pi}{\lambda}\Big(1 + \alpha k^2 + \dots\Big)\,, \tag{D.1a,b}$$

where the functions $X_n(\xi)$ and coefficients λ and α are to be found.

We substitute these expressions in to the governing equation (2.23) and boundary conditions (2.24a), (2.24b) and (2.26a) and expand in powers of k. We obtain

$$\begin{aligned}(1+k^2\xi^2)\left(X_0'' + k^2 X_2'' + \dots\right) + k^2\xi\left(X_0' + \dots\right) + 2k^2(1+\dots)\left(X_0 + \dots\right) \\ - \lambda^2(1 - 2\alpha k^2 + \dots)\big(X_0 + k^2 X_2 + \dots\big) = 0\,, \end{aligned} \tag{D.2}$$

subject to

$$X_0(0) + k^2 X_2(0) + \dots = 1\,, \qquad X_0'(0) + k^2 X_2'(0) + \dots = 0\,, \tag{D.3a,b}$$

$$X_0'(1) + k^2 X_2'(1) + \dots = (1 - k^2 + \dots)\big(X_0(1) + k^2 X_2(1) + \dots\big)\,. \tag{D.3c}$$

D.1 *The leading-order system for $X_0(\xi)$*

At $O(k^0)$, the governing equation (D.2) becomes

$$X_0'' - \lambda^2 X_0 = 0\,, \tag{D.4}$$

subject to

$$X_0(0) = 1\,, \qquad X_0'(0) = 0\,, \qquad X_0'(1) = X_0(1)\,, \tag{D.5a–c}$$

from (D.3).

The solution of (D.4) subject to (D.5a,b) is

$$X_0(\xi) = \cosh\lambda\xi\,. \tag{D.6}$$

Applying (D.5c) we find that we must have

$$\lambda = \coth\lambda\,. \tag{D.7}$$

This equation defines λ, and is the same condition as found by Cox & Jones (**4**). There is a single positive solution, which is found numerically to be

$$\lambda = 1.19968\ldots\,. \tag{D.8}$$

D.2 *The first-order system for $X_2(\xi)$*

At $O(k^2)$ the governing equation (D.2) becomes

$$\begin{aligned} X_2'' - \lambda^2 X_2 &= -\Big[\xi^2 X_0'' + \xi X_0 + 2X_0 + 2\alpha\lambda^2 X_0\Big] \\ &= -\Big[\lambda^2\xi^2\cosh\lambda\xi + \lambda\xi\sinh\lambda\xi + 2(1+\alpha\lambda^2)\cosh\lambda\xi\Big]\,, \end{aligned} \tag{D.9}$$

subject to

$$X_2(0) = 0\,, \qquad X_2'(0) = 0\,, \qquad X_2'(1) - X_2(1) = -X_0(1) = -\cosh\lambda\,, \tag{D.10a–c}$$

from (D.3).

From (D.10b) and the forcing in (D.9), X_2 must be even in ξ. Motivated by the complementary function for (D.9) and the inhomogeneous forcing, we seek a solution of the form

$$X_2(\xi) = A\xi^3\sinh\lambda\xi + B\xi^2\cosh\lambda\xi + C\xi\sinh\lambda\xi + D\cosh\lambda\xi\,. \tag{D.11}$$

To satisfy the equation (D.9) and the first boundary condition (D.10a), we find that we need to take

$$A = \frac{\lambda}{6}\,, \qquad B = 0\,, \qquad C = -\frac{1}{\lambda} - \alpha\lambda\,, \qquad D = 0\,. \tag{D.12a–d}$$

Applying the final boundary condition (D.10c), we obtain

$$\alpha = -\frac{2+\lambda^2}{6\lambda^2} = -0.39827\ldots \tag{D.13}$$

D.3 *Asymptotic expression for $\theta(\ell)$*

Using the value (D.13) for α in (D.1b) we have

$$\ell = \frac{n\pi}{\lambda}\left(1 - \frac{2+\lambda^2}{6\lambda^2}k^2 + O(k^4)\right) \tag{D.14}$$

Now

$$k = \frac{\theta}{\ell} = \frac{\lambda\theta}{n\pi}\Big(1 + O(k^2)\Big) = \frac{\lambda\theta}{n\pi}\Big(1 + O(\theta^2)\Big)\,. \tag{D.15}$$

Hence

$$\ell = \frac{n\pi}{\lambda}\left(1 - \frac{(2+\lambda^2)}{6n^2\pi^2}\theta^2 + O(\theta^4)\right)\,, \tag{D.16}$$

or alternatively

$$\theta = n\pi\sqrt{\frac{6}{2+\lambda^2}}\left(1 - \frac{\lambda\ell}{n\pi}\right)^{1/2} + O\left(\left(1 - \tfrac{\lambda\ell}{n\pi}\right)^{5/2}\right)\,. \tag{D.17}$$

APPENDIX E

Asymptotic solution for $k \ll 1$ when there is no area saving at the wall

Our numerical results suggest that as $k \to 0$ we have $\ell \to \infty$ and $\theta \to \theta_\infty$, a constant. To construct an asymptotic solution for $k \ll 1$, we therefore pose expansions of the form

$$X(\xi) = X_0(\xi) + k^2 X_2(\xi) + k^4 X_4(\xi) + \dots\,, \quad \ell = \frac{n\theta_\infty}{k}\left(1 + \alpha k^2 + \dots\right). \tag{E.1a,b}$$

We substitute these expressions in to the governing equation (2.23) and boundary conditions (2.24a,b) and (2.26a) and expand in powers of k. We obtain

$$\begin{aligned}(1+k^2\xi^2)\left(X_0'' + k^2 X_2'' + k^4 X_4'' + \dots\right) + k^2\xi\left(X_0' + k^2 X_2' + \dots\right)\\ + 2k^2(1 - k^2\xi^2 + \dots)\left(X_0 + k^2 X_2 + \dots\right)\\ - \frac{k^2\pi^2}{\theta_\infty^2}(1 - 2\alpha k^2 + \dots)\left(X_0 + k^2 X_2 + \dots\right) = 0\,,\end{aligned} \tag{E.2}$$

together with

$$X_0(0) + k^2 X_2(0) + \dots = 1\,, \quad X_0'(0) + k^2 X_2'(0) + \dots = 0\,, \quad X_0'(1) + k^2 X_2'(1) + \dots = 0\,. \tag{E.3a–c}$$

E.1 *The leading-order system for $X_0(\xi)$*

At $O(k^0)$, the governing equation and boundary conditions (E.2)–(E.3) become

$$X_0'' = 0\,, \tag{E.4}$$

subject to

$$X_0(0) = 1\,, \qquad X_0'(0) = 0\,, \qquad X_0'(1) = 0\,. \tag{E.5a–c}$$

Despite there being too many boundary conditions, there is solution of (E.4) which satisfies all of (E.5), namely

$$X_0(\xi) = 1\,. \tag{E.6}$$

The ability to find a solution to this over-determined system validates the proposed form (E.1) of our asymptotic expansion.

E.2 *The first-order system for $X_2(\xi)$*

At $O(k^2)$ the governing equation and boundary conditions (E.2)–(E.3) become

$$X_2'' = -\left[\xi^2 X_0'' + \xi X_0' + 2X_0 - \frac{\pi^2}{\theta_\infty^2} X_0\right] = \frac{\pi^2}{\theta_\infty^2} - 2\,, \tag{E.7}$$

subject to

$$X_2(0) = 0\,, \qquad X_2'(0) = 0\,, \qquad X_2'(1) = 0\,. \tag{E.8a–c}$$

By integrating (E.7) and applying (E.8), we see that the system has a solution if and only if θ_∞ takes a specific value. We find

$$\theta_\infty = \frac{\pi}{\sqrt{2}}\,, \qquad X_2(\xi) = 0\,. \tag{E.9a,b}$$

E.3 *The second-order system for $X_4(\xi)$*

At $O(k^4)$ governing equation and boundary conditions (E.2)–(E.3) become

$$X_4'' = -\left[\xi^2 X_2'' + \xi X_2' + 2X_2 - \frac{\pi^2}{\theta_\infty^2} X_2\right] - \left[-2\xi^2 X_0 + \frac{2\alpha\pi^2}{\theta_\infty^2} X_0\right]$$
$$= 4\alpha - 2\xi^2\,, \tag{E.10}$$

subject to

$$X_4(0) = 0\,, \qquad X_4'(0) = 0\,, \qquad X_4'(1) = 0\,. \tag{E.11a–c}$$

By integrating (E.10) and applying (E.11), we see that the system has a solution if and only if α takes a specific value. We find

$$\alpha = \frac{1}{6}\,, \qquad X_4(\xi) = -\frac{\xi^2(2-\xi^2)}{6}\,. \tag{E.12a,b}$$

E.4 *Asymptotic expression for $\theta(\ell)$*

Using the value (E.12a) for α in (E.1b) we have

$$\theta = k\ell = \frac{n\pi}{\sqrt{2}}\left(1 + \frac{1}{6}k^2 + O(k^4)\right) \tag{E.13}$$

Now

$$k = \frac{\theta}{\ell} = \frac{n\pi}{\sqrt{2}\,\ell}\Big(1 + O(k^2)\Big) = \frac{n\pi}{\sqrt{2}\,\ell}\Big(1 + O(\ell^{-2})\Big)\,. \tag{E.14}$$

Finally, using (E.14) to eliminate k from (E.13), we obtain

$$\theta = \frac{n\pi}{\sqrt{2}}\left(1 + \frac{n^2\pi^2}{12\,\ell^2} + O(\ell^{-4})\right)\,. \tag{E.15}$$

APPENDIX F

Sums of singular-line displacements for multiple vanes

In this appendix, we derive the results quoted in (4.22) and (4.26) for the sums of $h_n^{(j)}$, $q_n^{(j)}$ and $h_n^{(j)2}$ over multiple equally-spaced vanes. We evaluate the sums by expressing the trigonometric functions as the real ($\Re$) or imaginary ($\Im$) part of a complex exponential, and then summing the resulting geometric progression.

Inserting the Fourier series (4.13) and (4.14) into the expressions (4.3) and (4.4) for $h^{(j)}$ and $q^{(j)}$ and equating coefficients, we obtain

$$q_n^{(j)} = q_n^{(0)}\,\cos\theta_j + h_n^{(0)}\,\sin\theta_j\,, \tag{F.1}$$
$$h_n^{(j)} = -q_n^{(0)}\,\sin\theta_j + h_n^{(0)}\,\cos\theta_j \tag{F.2}$$

where the angle of the jth vane is given by $\theta_j = 2j\pi/N$.

F.1 *Sums of $h_n^{(j)}$ and $q_n^{(j)}$*

For the evaluation of $\sum_{j=0}^{N-1} h_n^{(j)}$ and $\sum_{j=0}^{N-1} q_n^{(j)}$, we need the following sums of trigonometric functions:

$$\sum_{j=0}^{N-1}\cos\theta_j = \Re\left(\sum_{j=0}^{N-1} \mathrm{e}^{2\pi\mathrm{i}j/N}\right) = \Re\left(\frac{\mathrm{e}^{2\pi\mathrm{i}}-1}{\mathrm{e}^{2\pi\mathrm{i}/N}-1}\right) = 0\,, \tag{F.3}$$

$$\sum_{j=0}^{N-1}\sin\theta_j = \Im\left(\sum_{j=0}^{N-1} \mathrm{e}^{2\pi\mathrm{i}j/N}\right) = \Im\left(\frac{\mathrm{e}^{2\pi\mathrm{i}}-1}{\mathrm{e}^{2\pi\mathrm{i}/N}-1}\right) = 0\,, \tag{F.4}$$

which hold for all integer values of $N \geq 2$. Summing (F.1) and (F.2) over j, and using (F.3) and (F.4), we obtain the two results quoted in (4.22).

F.2 *Sum of* $h_n^{(j)\,2}$

For the evaluation of $\sum_{j=0}^{N-1} h_n^{(j)\,2}$, we need the following sums of trigonometric functions. For integers $N > 2$ we can write:

$$2\sum_{j=0}^{N-1}\cos^2\theta_j = \sum_{j=0}^{N-1}\Big(1+\cos 2\theta_j\Big) = N + \Re\left(\sum_{j=0}^{N-1}\mathrm{e}^{4\pi\mathrm{i}j/N}\right) = N + \Re\left(\frac{\mathrm{e}^{4\pi\mathrm{i}}-1}{\mathrm{e}^{4\pi\mathrm{i}/N}-1}\right) = N\,, \tag{F.5}$$

$$2\sum_{j=0}^{N-1}\sin^2\theta_j = \sum_{j=0}^{N-1}\Big(1-\cos 2\theta_j\Big) = N - \Re\left(\sum_{j=0}^{N-1}\mathrm{e}^{4\pi\mathrm{i}j/N}\right) = N - \Im\left(\frac{\mathrm{e}^{4\pi\mathrm{i}}-1}{\mathrm{e}^{4\pi\mathrm{i}/N}-1}\right) = N\,, \tag{F.6}$$

$$2\sum_{j=0}^{N-1}\sin\theta_j\cos\theta_j = \sum_{j=0}^{N-1}\sin 2\theta_j = \Im\left(\sum_{j=0}^{N-1}\mathrm{e}^{4\pi\mathrm{i}j/N}\right) = \Im\left(\frac{\mathrm{e}^{4\pi\mathrm{i}}-1}{\mathrm{e}^{4\pi\mathrm{i}/N}-1}\right) = 0\,. \tag{F.7}$$

When $N = 2$, we instead obtain

$$\sum_{j=0}^{N-1}\cos^2\theta_j = 2\,, \qquad \sum_{j=0}^{N-1}\sin^2\theta_j = 0\,, \qquad \sum_{j=0}^{N-1}\sin\theta_j\cos\theta_j = 0\,. \tag{F.8a–c}$$

Squaring (F.2), and summing over j, we have

$$\sum_{j=0}^{N-1} h_n^{(j)\,2} = q_n^{(0)\,2}\sum_{j=0}^{N-1}\sin^2\theta_j - 2q_n^{(0)}h_n^{(0)}\sum_{j=0}^{N-1}\sin\theta_j\cos\theta_j + h_n^{(0)\,2}\sum_{j=0}^{N-1}\cos^2\theta_j\,. \tag{F.9}$$

Then, using (F.5)–(F.8), we obtain the result quoted in (4.26).